
Spectral embedding for dynamic networks with stability guarantees

Ian Gallagher

University of Bristol, UK
ian.gallagher@bristol.ac.uk

Andrew Jones

University of Bristol, UK
andrew.jones@bristol.ac.uk

Patrick Rubin-Delanchy

University of Bristol, UK
patrick.rubin-delanchy@bristol.ac.uk

Abstract

We consider the problem of embedding a dynamic network, to obtain time-evolving vector representations of each node, which can then be used to describe changes in behaviour of individual nodes, communities, or the entire graph. Given this open-ended remit, we argue that two types of stability in the spatio-temporal positioning of nodes are desirable: to assign the same position, up to noise, to nodes behaving similarly at a given time (cross-sectional stability) and a constant position, up to noise, to a single node behaving similarly across different times (longitudinal stability). Similarity in behaviour is defined formally using notions of exchangeability under a dynamic latent position network model. By showing how this model can be recast as a multilayer random dot product graph, we demonstrate that unfolded adjacency spectral embedding satisfies both stability conditions. We also show how two alternative methods, omnibus and independent spectral embedding, alternately lack one or the other form of stability.

1 Introduction

Consider a dynamic network in which nodes come and go, change abruptly or evolve, alone or in communities, and form connections accordingly. Our goal is to find a vector representation, $\hat{\mathbf{Y}}_i^{(t)} \in \mathbb{R}^d$, for every node i and time t , which could be used for a diversity of downstream analyses, such as clustering, time series analysis, classification, model selection and more. This problem is known as dynamic (or evolutionary) network (or graph) embedding, and a great number of scalable and empirically successful techniques have been put forward, with recent surveys by [47, 51]. We consider, among these, a subset about which it is reasonable to try to establish a certain statistical guarantee.

The novelty of this paper is *not* to propose a new procedure. Instead, it is to demonstrate that an existing procedure, unfolded adjacency spectral embedding (UASE) [17], has two important stability properties. Given a sequence of symmetric adjacency matrices $\mathbf{A}^{(1)}, \dots, \mathbf{A}^{(T)} \in \{0, 1\}^{n \times n}$, where $\mathbf{A}_{ij}^{(t)} = 1$ if nodes i and j form an edge at time t , UASE computes the rank d matrix factorisation of $\mathbf{A} := (\mathbf{A}^{(1)} | \dots | \mathbf{A}^{(T)})$ to obtain $\mathbf{A} \approx \hat{\mathbf{X}} \hat{\mathbf{Y}}^\top$ using the singular value decomposition (precise details later). The matrix $\hat{\mathbf{Y}} \in \mathbb{R}^{nT \times d}$ contains, as rows, the desired representations $\hat{\mathbf{Y}}_1^{(1)}, \dots, \hat{\mathbf{Y}}_n^{(1)}, \dots, \hat{\mathbf{Y}}_1^{(T)}, \dots, \hat{\mathbf{Y}}_n^{(T)}$.

The original motivation for UASE was to analyse multilayer (or multiplex) graphs under an appropriate extension of the random dot product graph model [17]. To evaluate UASE and other procedures on the task of dynamic network embedding, we instead consider the dynamic latent position model

$$\mathbf{A}_{ij}^{(t)} \stackrel{\text{ind}}{\sim} \text{Bernoulli} \left(f \left\{ \mathbf{Z}_i^{(t)}, \mathbf{Z}_j^{(t)} \right\} \right), \quad (1)$$

for $1 \leq i < j \leq n$, $t \in [T]$, where $\mathbf{Z}_i^{(t)} \in \mathbb{R}^k$ represents the unknown position of node i at time t , and $f : \mathbb{R}^k \times \mathbb{R}^k \rightarrow [0, 1]$ is a symmetric function.

This model is well-established [39, 22, 15, 16, 33, 23, 9, 43, 11, 10], with recent reviews by [20] and [45], and inference usually proceeds on the basis of a parametric model for f (e.g. logistic in the latent position distance [39]) and for the dynamics of $\mathbf{Z}_i^{(t)}$ (e.g. a Markov process [39]). The model also includes the dynamic degree-corrected, mixed-membership and standard stochastic block models as special cases, which were studied in [48, 52, 14, 29, 50, 49, 31, 4, 32, 19].

To make statistical sense of UASE under this latent position model, we must somehow connect its output $\hat{\mathbf{Y}}_i^{(t)}$ to $\mathbf{Z}_i^{(t)}$. To this end we construct a canonical representative of $\mathbf{Z}_i^{(t)}$, denoted $\mathbf{Y}_i^{(t)}$, that UASE can be seen to estimate. Although we make some regularity assumptions on f and the $\mathbf{Z}_i^{(t)}$, they are not modelled in an explicit, parametric way, and UASE can clearly be used in practice without having a specific model in mind. For example, we do not make a Markovian assumption on the evolution of $\mathbf{Z}_i^{(t)}$ and UASE can be used to uncover periodic behaviours.

The key purpose of imposing a dynamic latent position model is to allow us to put down certain embedding stability requirements. Using this framework, we can define precisely what we mean by two nodes, i and j , behaving “similarly” at times s and t respectively. In such cases, ideally we would have $\hat{\mathbf{Y}}_i^{(s)} \approx \hat{\mathbf{Y}}_j^{(t)}$. Two special cases are: to assign the same position, up to noise, to nodes behaving similarly at a given time (cross-sectional stability) and a constant position, up to noise, to a single node behaving similarly across different times (longitudinal stability).

To achieve both cross-sectional and longitudinal stability is generally elusive. We show that two plausible alternatives, omnibus [26] and independent embedding of each $\mathbf{A}^{(t)}$, alternately exhibit one form of stability and not the other. More generally, we find existing procedures [6, 27, 40, 8, 54, 7, 28, 5, 4, 32, 37, 19] tend to trade one type of stability off against the other, e.g. via user-specified cost functions. As a side-note, it could be observed that omnibus embedding is not being evaluated on a task for which it was designed, since in the theory of [26] the graphs are identically distributed. Because the technique is so different from the others, we still feel it makes an interesting addition.

Our central contribution is to prove that UASE asymptotically provides both longitudinal and cross-sectional stability: for two nodes, i and j , behaving similarly at times s and t respectively, we have $\hat{\mathbf{Y}}_i^{(s)} \approx \hat{\mathbf{Y}}_j^{(t)}$ and, moreover, $\hat{\mathbf{Y}}_i^{(s)}$ and $\hat{\mathbf{Y}}_j^{(t)}$ have asymptotically equal error distribution. We emphasise that these properties hold without requiring any sort of global stability — the network could vary wildly over time but certain nodes still stay fixed. In the asymptotic regime considered, we have $n \rightarrow \infty$, but T fixed so that, for example, our results are relevant to the case of two large graphs. The alternative regime where $T \rightarrow \infty$ grows but n is fixed is not easily handled by existing theory and to provide constant updates to UASE (or omnibus embedding) in a streaming context presents significant computational challenges.

The remainder of this article is structured as follows. Section 2 gives a pedagogical example demonstrating the cross-sectional and longitudinal stability of UASE in a two-step dynamic stochastic block model, while highlighting the instability of omnibus and independent spectral embedding. In Section 3, we prove a central limit theorem for UASE under a dynamic latent position model, and demonstrate that the distribution satisfies both stability conditions. In Section 4, we review the stability of other dynamic network embedding procedures. Section 5 presents an example of UASE applied to a dynamic network of social interactions in a French primary school, with a dynamic community detection example given in the main text and a further classification example provided in the Appendix. Section 6 concludes.

2 Motivating example

Suppose it is of interest to uncover dynamic community structure, including communities changing, merging or splitting. The dynamic stochastic block model [52, 50] provides a simple explicit model for this, in which two nodes connect at a certain point in time with probability only dependent on their current community membership. Suppose that at times 1 and 2, we have the following inter-community link probability matrices,

$$\mathbf{B}^{(1)} = \begin{pmatrix} 0.08 & 0.02 & 0.18 & 0.10 \\ 0.02 & 0.20 & 0.04 & 0.10 \\ 0.18 & 0.04 & 0.02 & 0.02 \\ 0.10 & 0.10 & 0.02 & 0.06 \end{pmatrix}, \quad \mathbf{B}^{(2)} = \begin{pmatrix} 0.16 & 0.16 & 0.04 & 0.10 \\ 0.16 & 0.16 & 0.04 & 0.10 \\ 0.04 & 0.04 & 0.09 & 0.02 \\ 0.10 & 0.10 & 0.02 & 0.06 \end{pmatrix}.$$

At time 1 there are four communities present, for example, a node of community 1 connects with a node of community 3 with probability 0.18. At time 2, this matrix changes so that communities 1 and 2 have merged, community 3 has moved, whereas community 4 is unchanged. For simplicity, in this example, the community membership of each node is fixed across time-steps.

We simulate a dynamic network from this model over these two time steps, on $n = 1000$ nodes, equally divided among the four communities and investigate the results of three embedding techniques: UASE, omnibus, and independent spectral embedding, displayed in Figure 1. Note that the different techniques produce embeddings of different dimensions; UASE embeds into $d = 4$ dimensions, omnibus embedding $\tilde{d} = 7$, while independent spectral embedding has $d_1 = 4$ and $d_2 = 3$. For visualisation, we show the leading two dimensions for each embedding. Given the dynamics described above, we contend that the following properties would be desirable:

1. *Cross-sectional stability*: The embeddings for communities 1 and 2 at time 2 are close.
2. *Longitudinal stability*: The embeddings for community 4 at times 1 and 2 are close.

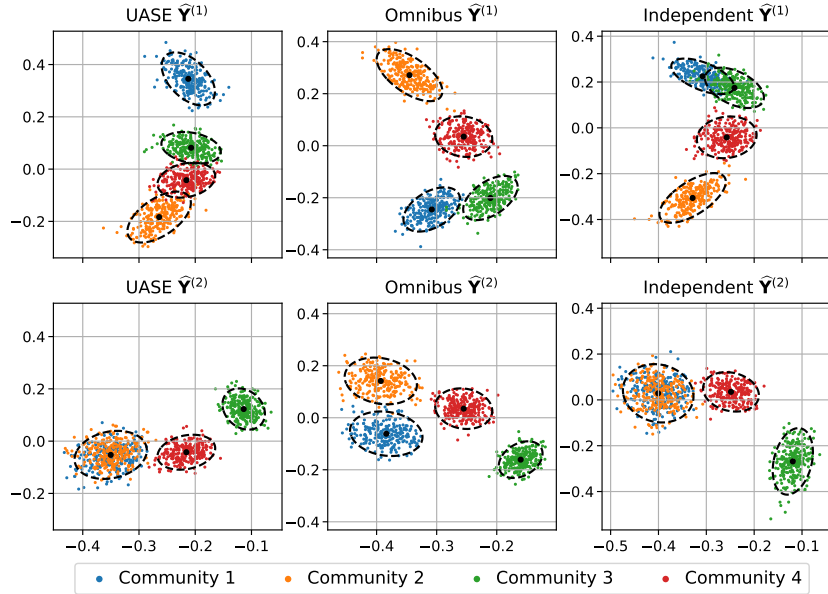


Figure 1: First two dimensions of the embeddings for the adjacency matrices $\mathbf{A}^{(1)}$ and $\mathbf{A}^{(2)}$ using three different techniques: UASE, omnibus and separate embedding. The points are coloured according to true community membership, with the black dots showing the fitted community centroid and the ellipses a fitted 95% level Gaussian contour.

Figure 1 illustrates that UASE has both properties: the blue and orange point clouds merge at time 2, and the red point cloud has the same location *and* shape over the two time points. On the other hand, omnibus embedding only has longitudinal stability (the blue and orange point clouds don't merge at

time 2), whereas independent spectral embedding only has cross-sectional stability (the red point cloud is at different locations over the two time points).

3 Theoretical background and results

We consider a sequence of random graphs distributed according to a dynamic latent position model, in which the latent position sequences $(\mathbf{Z}_i^{(t)})_{t \in [T]}$ (where we use the shorthand $[T] = \{1, \dots, T\}$) are independent of each other, and identically distributed according to a joint distribution \mathcal{F} on \mathcal{Z}^T , for a bounded subset \mathcal{Z} of \mathbb{R}^k . We emphasise that for a fixed i the latent positions $\mathbf{Z}_i^{(t)}$ and $\mathbf{Z}_i^{(t')}$ may have different distributions — we are imposing exchangeability over the nodes (invariance to node labelling), but not over time.

By extending the function f to be zero outside of its domain of definition, we may view it as an element of $L^2(\mathbb{R}^k \times \mathbb{R}^k)$, and consequently may define a compact, self-adjoint operator A on $L^2(\mathbb{R}^k)$ by setting

$$Ag(x) = \int_{\mathbb{R}^k} f(x, y)g(y)dy \quad (2)$$

for all $g \in L^2(\mathbb{R}^k)$. The operator A has a—possibly infinite—sequence of non-zero eigenvalues $\lambda_1 \geq \lambda_2 \geq \dots$ with corresponding orthonormal eigenfunctions $u_1, u_2, \dots \in L^2(\mathbb{R}^k)$, such that $Au_j = \lambda_j u_j$ (for further details, see for example [35]). We shall make the simplifying assumption that A has a *finite* number of non-zero eigenvalues, in which case f admits a canonical eigendecomposition

$$f(\mathbf{x}, \mathbf{y}) = \sum_{i=1}^D \lambda_i u_i(\mathbf{x})u_i(\mathbf{y}), \quad (3)$$

assumed to hold everywhere, where after relabelling we may assume that $|\lambda_1| \geq \dots \geq |\lambda_D|$.

Several families of functions satisfy the finite rank assumption $D < \infty$, such as the multivariate polynomials [35]. Moreover, several existing statistical models can be written as dynamic latent position network models in which $D < \infty$, including the dynamic mixed membership, degree-corrected, and standard stochastic block models. To assume $D < \infty$, more generally, is tantamount to a claim that, for large n , $\mathbf{A}^{(t)}$ has ‘low’ approximate rank: an overwhelming proportion of its eigenvalues are close to zero. Large matrices with low approximate rank are routinely encountered across numerous disciplines, and the study [46] provides a hypothesis for this “puzzling” general observation. However, given a real network, we might reject the hypothesis that f has low rank (we must then also reject any type of stochastic block model), for example on the basis of triangle counts [41]. In such a setting, we anticipate that UASE is still consistent and stable if d is allowed to grow sufficiently slowly with n and there exist asymptotic results for adjacency spectral embedding, for the single graph case, showing convergence in Wasserstein distance under assumptions on eigenvalue decay which can be related to the smoothness of f [24]. However, even if we could obtain such results for UASE, they would not be as powerful as those we present here for the finite rank case, where we show uniform consistency with asymptotic Gaussian error.

Theorem 1. The adjacency matrices $\mathbf{A}^{(1)}, \dots, \mathbf{A}^{(T)}$ are jointly distributed according to a multilayer random dot product graph model.

The multilayer random dot product graph model (MRDPG, see [17]) is a multi-graph analogue of the generalised random dot product graph model [36], and is characterised by the existence of matrices $\mathbf{\Lambda}^{(t)} \in \mathbb{R}^{d \times d_t}$ and random matrices $\mathbf{X} \in \mathbb{R}^{n \times d}$ and $\mathbf{Y}^{(t)} \in \mathbb{R}^{n \times d_t}$ (generated according to some joint distribution \mathcal{G}) such that

$$\mathbf{A}_{ij}^{(t)} \stackrel{\text{ind}}{\sim} \text{Bernoulli}(\mathbf{X}_i \mathbf{\Lambda}^{(t)} \mathbf{Y}_j^{(t)\top}) \quad (4)$$

for each $t \in [T]$ and $i, j \in [n]$, where \mathbf{X}_i and $\mathbf{Y}_j^{(t)}$ denote the i th and j th rows of \mathbf{X} and $\mathbf{Y}^{(t)}$ respectively.

We refer the reader to the supplemental material for full details of the proof of Theorem 1, but note that given knowledge of the function f and the underlying distribution \mathcal{F} we can construct explicit

maps $\varphi : \mathbb{R}^{Tk} \rightarrow \mathbb{R}^d$ and $\varphi_t : \mathbb{R}^k \rightarrow \mathbb{R}^{d_t}$, producing row vectors, and matrices $\mathbf{A}^{(t)} \in \mathbb{R}^{d \times d_t}$ such that

$$f(\mathbf{Z}_i^{(t)}, \mathbf{Z}_j^{(t)}) = \mathbf{X}_i \mathbf{A}^{(t)} \mathbf{Y}_j^{(t)\top}, \quad (5)$$

where $\mathbf{X}_i = \varphi(\mathbf{Z}_i)$, $\mathbf{Y}_j^{(t)} = \varphi_t(\mathbf{Z}_j^{(t)})$ and $\mathbf{Z}_i = (\mathbf{Z}_i^{(1)} | \dots | \mathbf{Z}_i^{(T)}) \in \mathbb{R}^{Tk}$, for each $t \in [T]$ and $i, j \in [n]$. Consequently, each Gram matrix

$$\mathbf{P}^{(t)} = (f(\mathbf{Z}_i^{(t)}, \mathbf{Z}_j^{(t)}))_{i,j \in [n]} \quad (6)$$

admits a factorisation into a product of low-rank matrices, in which the matrix whose rows are the vectors $\varphi(\mathbf{Z}_i)$ appears as a common factor. The dimensions d_t and d are precisely the ranks of the matrices $\mathbf{P}^{(t)}$ and their concatenation $\mathbf{P} = (\mathbf{P}^{(1)} | \dots | \mathbf{P}^{(T)})$ respectively. In the theory that follows we will assume that the dimension d is known and fixed, whereas in practice we would usually have to estimate it (for example by using profile likelihood [55]).

We can extend our model to incorporate a range of sparsity regimes by scaling the function f by a sparsity factor ρ_n , which we assume is either constant and equal to 1, or else tends to zero as n grows, corresponding to dense and sparse regimes respectively. When this factor is present, the maps φ and φ_t are scaled by a factor of $\rho_n^{1/2}$.

Realising our model as an MRDPG allows us to make precise statements about the asymptotic behaviour of the point clouds obtained through UASE. In particular, it is the existence of a common factor in the decomposition of each of the Gram matrices $\mathbf{P}^{(t)}$ that gives rise to the stability properties previously demonstrated in the embeddings $\hat{\mathbf{Y}}^{(t)}$, as this matrix in a sense acts as an anchor for the individual point clouds.

In [17] UASE is used to obtain *two* multi-graph embeddings; the algorithm below retains only one — the ‘dynamic’ component.

Algorithm 1 Unfolded adjacency spectral embedding for dynamic networks

- input** symmetric adjacency matrices $\mathbf{A}^{(1)}, \dots, \mathbf{A}^{(T)} \in \{0, 1\}^{n \times n}$, embedding dimension d
- 1: Form the matrix $\mathbf{A} = (\mathbf{A}^{(1)} | \dots | \mathbf{A}^{(T)}) \in \{0, 1\}^{n \times Tn}$ (column concatenation)
 - 2: Compute the truncated singular value decomposition $\mathbf{U}_\mathbf{A} \Sigma_\mathbf{A} \mathbf{V}_\mathbf{A}^\top$ of \mathbf{A} , where $\Sigma_\mathbf{A}$ contains the d largest singular values of \mathbf{A} , and $\mathbf{U}_\mathbf{A}, \mathbf{V}_\mathbf{A}$ the corresponding left and right singular vectors
 - 3: Compute the right embedding $\hat{\mathbf{Y}} = \mathbf{V}_\mathbf{A} \Sigma_\mathbf{A}^{1/2} \in \mathbb{R}^{Tn \times d}$ and create sub-embeddings $\hat{\mathbf{Y}}^{(t)} \in \mathbb{R}^{n \times d}$ where $\hat{\mathbf{Y}} = (\hat{\mathbf{Y}}^{(1)}; \dots; \hat{\mathbf{Y}}^{(T)})$ (row concatenation)
- return** node embeddings for each time period $\hat{\mathbf{Y}}^{(1)}, \dots, \hat{\mathbf{Y}}^{(T)}$
-

Replacing \mathbf{A} with \mathbf{P} in this construction yields the *noise-free* embeddings $\tilde{\mathbf{Y}}^{(t)}$, whose rows are known to be linear transformations of the vectors $\varphi_t(\mathbf{Z}_i^{(t)})$ (see the supplemental material for further details). A desirable property of UASE is that since the matrices $\mathbf{A}^{(t)}$ follow an MRDPG model there exist known asymptotic distributional results for the embeddings $\hat{\mathbf{Y}}^{(t)}$. In order to ensure the validity of these results, we will make the assumption that the sparsity factor ρ_n satisfies $\rho_n = \omega(n^{-1} \log^c(n))$ for some universal constant $c > 1$.

In the results to follow, UASE is shown to be consistent and stable in a uniform sense, i.e. the maximum error of any position estimate goes to zero, under the assumption that the average network degree grows polylogarithmically in n . To achieve this for less than logarithmic growth would be impossible, by any algorithm, because it would violate the information-theoretic sparsity limit for perfect community recovery under the stochastic block model [1]. In practice this means that the embedding will have high variance when the graphs have few edges. Several approaches have been proposed to make single graph embeddings more robust (e.g. to sparsity or heterogeneous degrees), such as based on the regularised Laplacian [3] or non-backtracking matrices [21], but it is an open and interesting question how to extend them to the dynamic graph setting to achieve both cross-sectional and longitudinal stability.

The first of our distributional results states that after applying an orthogonal transformation—which leaves the structure of the resulting point cloud intact—the embedded points $\hat{\mathbf{Y}}_i^{(t)}$ converge in the Euclidean norm to the noise-free embedded points $\tilde{\mathbf{Y}}_i^{(t)}$ as the graph size grows:

Proposition 2. There exists a sequence of orthogonal matrices $\tilde{\mathbf{W}} \in O(d)$ such that

$$\max_{i \in \{1, \dots, n\}} \|\hat{\mathbf{Y}}_i^{(t)} \tilde{\mathbf{W}} - \tilde{\mathbf{Y}}_i^{(t)}\| = O\left(\frac{\log^{1/2}(n)}{\rho_n^{1/2} n^{1/2}}\right) \quad (7)$$

with high probability for each t .

The matrices $\tilde{\mathbf{W}}$ are unidentifiable in practice, but are defined to be the solution to the one-mode orthogonal Procrustes problem

$$\tilde{\mathbf{W}} = \arg \min_{\mathbf{Q} \in O(d)} \|\mathbf{U}_A \mathbf{Q} - \mathbf{U}_P\|_F^2 + \|\mathbf{V}_A \mathbf{Q} - \mathbf{V}_P\|_F^2, \quad (8)$$

where $\|\cdot\|_F^2$ denotes the Frobenius norm. We emphasise that the matrix $\tilde{\mathbf{W}}$ is *the same* for each embedding, and so similar behaviour in the noise-free embeddings $\tilde{\mathbf{Y}}^{(t)}$ is captured by UASE.

Our second result states that after applying a *second* orthogonal transformation the above error converges in distribution to a fixed multivariate Gaussian distribution:

Proposition 3. Let $\zeta = (\zeta_1 | \dots | \zeta_T) \sim \mathcal{F}$, and for $\mathbf{z} \in \mathcal{Z}$ define

$$\Sigma_t(\mathbf{z}) = \begin{cases} \mathbb{E}_\zeta \left[f(\mathbf{z}, \zeta_t) (1 - f(\mathbf{z}, \zeta_t)) \cdot \varphi(\zeta)^\top \varphi(\zeta) \right] & \text{if } \rho_n = 1 \\ \mathbb{E}_\zeta \left[f(\mathbf{z}, \zeta_t) \cdot \varphi(\zeta)^\top \varphi(\zeta) \right] & \text{if } \rho_n \rightarrow 0. \end{cases} \quad (9)$$

Then there exists a deterministic matrix $\mathbf{R}_* \in \mathbb{R}^{d \times d}$ and a sequence of orthogonal matrices $\mathbf{W} \in O(d)$ such that, given $\mathbf{z} \in \mathcal{Z}$, for all $\mathbf{y} \in \mathbb{R}^d$ and for any fixed $i \in [n]$ and $t \in [T]$,

$$\mathbb{P}\left(n^{1/2}(\hat{\mathbf{Y}}_i^{(t)} \tilde{\mathbf{W}} - \tilde{\mathbf{Y}}_i^{(t)}) \mathbf{W} \leq \mathbf{y} \mid \mathbf{Z}_i^{(t)} = \mathbf{z}\right) \rightarrow \Phi(\mathbf{y}, \mathbf{R}_* \Sigma_t(\mathbf{z}) \mathbf{R}_*^\top). \quad (10)$$

As in our previous results, the matrices \mathbf{W} and \mathbf{R}_* can be explicitly constructed given knowledge of the underlying function f and distribution \mathcal{F} (again, we defer full details to the supplemental material). Note that as in Proposition 2, both constructed matrices are common to *all* embeddings.

We can now demonstrate one of the key advantages that UASE holds over other embedding methods, namely that *UASE exhibits both cross-sectional and longitudinal stability*, in a sense that we shall now define. We say that two space-time positions (\mathbf{z}, t) and (\mathbf{z}', t') are *exchangeable* if $f(\mathbf{z}, \zeta_t) = f(\mathbf{z}', \zeta_{t'})$ with probability one, where $\zeta = (\zeta_1 | \dots | \zeta_T) \sim \mathcal{F}$, and that the positions are *exchangeable up to degree* if $f(\mathbf{z}, \zeta_t) = \alpha f(\mathbf{z}', \zeta_{t'})$ for some $\alpha > 0$. Equivalently, (\mathbf{z}, t) and (\mathbf{z}', t') are exchangeable if conditional on $\mathbf{Z}_i^{(t)} = \mathbf{z}$ and $\mathbf{Z}_j^{(t')} = \mathbf{z}'$ the i th row of $\mathbf{P}^{(t)}$ and j th row of $\mathbf{P}^{(t')}$ are equal with probability one.

Definition 4. Given a generic method for dynamic network embedding, with output denoted $(\hat{\mathbf{Z}}_i^{(t)})_{i \in [n]; t \in [T]}$, define the following stability properties:

1. *Cross-sectional stability:* Given exchangeable (\mathbf{z}, t) and (\mathbf{z}', t) , $\hat{\mathbf{Z}}_i^{(t)}$ and $\hat{\mathbf{Z}}_j^{(t)}$ are asymptotically equal, with identical error distribution, conditional on $\mathbf{Z}_i^{(t)} = \mathbf{z}$ and $\mathbf{Z}_j^{(t)} = \mathbf{z}'$.
2. *Longitudinal stability:* Given exchangeable (\mathbf{z}, t) and (\mathbf{z}, t') , $\hat{\mathbf{Z}}_i^{(t)}$ and $\hat{\mathbf{Z}}_i^{(t')}$ are asymptotically equal, with identical error distribution, conditional on $\mathbf{Z}_i^{(t)} = \mathbf{Z}_i^{(t')} = \mathbf{z}$.

The following result then shows that UASE exhibits both types of stability:

Corollary 5. Conditional on $\mathbf{Z}_i^{(t)} = \mathbf{z}$ and $\mathbf{Z}_j^{(t')} = \mathbf{z}'$, the following properties hold:

1. If (\mathbf{z}, t) and (\mathbf{z}', t') are exchangeable then $\hat{\mathbf{Y}}_i^{(t)}$ and $\hat{\mathbf{Y}}_j^{(t')}$ are asymptotically equal, with identical error distribution.
2. If (\mathbf{z}, t) and (\mathbf{z}', t') are exchangeable up to degree then $\hat{\mathbf{Y}}_i^{(t)}$ and $\alpha \hat{\mathbf{Y}}_j^{(t')}$ are asymptotically equal and, under a sparse regime, their error distributions are equal up to scale, satisfying $\Sigma_t(\mathbf{z}) = \alpha \Sigma_{t'}(\mathbf{z}')$.

We can gain insight into our theoretical results by applying them in the context of common statistical models. Under the dynamic stochastic block model of Section 2, a pair (\mathbf{z}, t) and (\mathbf{z}', t') are

exchangeable if and only if the corresponding rows of $\mathbf{B}^{(t)}$ and $\mathbf{B}^{(t')}$ are identical. Proposition 3 then predicts that the point cloud obtained via UASE should decompose into a finite number of *Gaussian* clusters, as we observe in Figure 1. Moreover, when combined with Corollary 5 the equality of the fourth rows of $\mathbf{B}^{(1)}$ and $\mathbf{B}^{(2)}$ implies that we should expect *identical* clusters (centre and shape) corresponding to the fourth community at both time points (indicating longitudinal stability) and similarly the equality of the first and second rows of $\mathbf{B}^{(2)}$ tells us that the communities should be indistinguishable at the second time point (indicating cross-sectional stability), behaviours we observe in Figure 1. Under degree-correction [18, 29], Corollary 5 indicates that we should at least observe cross-sectional and longitudinal stability along ‘rays’ representing communities, a behaviour that is exhibited in Figure 2.

4 Comparison

In this section we investigate the stability properties of alternatives to UASE. Table 1 shows the stability of the three embedding algorithms described in Section 2 and two wider classes of algorithms, described below. For alternatives to UASE, it will be considered sufficient to establish whether an embedding is stable when applied to the Gram matrices $\mathbf{P}^{(1)}, \dots, \mathbf{P}^{(T)}$. A method found to be unstable in this noise-free condition is not expected to be stable when the matrices are replaced by their noisy observations $\mathbf{A}^{(1)}, \dots, \mathbf{A}^{(T)}$.

Table 1: Classes of dynamic network embedding algorithms: a brief description, the algorithm complexity and its cross-sectional/longitudinal stability. In the three latter classes, one may replace $\mathbf{A}^{(t)}$ with other matrix representations of the graph (e.g. the normalised Laplacian). Further details in main text.

Algorithm	Description	Complexity	Stability
UASE [17]	Embed $\mathbf{A} = (\mathbf{A}^{(1)} \dots \mathbf{A}^{(T)})$	$O(dTn^2)$	Both
Omnibus [26]	Embed $\tilde{\mathbf{A}}; \tilde{\mathbf{A}}_{s,t} = (\mathbf{A}^{(s)} + \mathbf{A}^{(t)})/2$	$O(\tilde{d}T^2n^2)$	Longitudinal
Independent	Embed $\mathbf{A}^{(t)}$	$O(\sum_t d_t n^2)$	Cross-sectional
Separate embedding [40, 8, 4, 32, 37, 19]	Embed $\bar{\mathbf{A}}^{(t)} = \sum_k w_k \mathbf{A}^{(t-k)}$		Neither
Joint embedding [27, 7, 54, 5, 28]	$\arg \min_{\hat{\mathbf{Y}}^{(1)}, \dots, \hat{\mathbf{Y}}^{(T)}} \alpha \sum_t \text{CS}(\hat{\mathbf{Y}}^{(t)}, \mathbf{A}^{(t)})$ $+ (1 - \alpha) \sum_t \text{CT}(\hat{\mathbf{Y}}^{(t)}, \hat{\mathbf{Y}}^{(t+1)})$		Neither

The omnibus method computes the spectral embedding of the matrix $\tilde{\mathbf{A}} \in \{0, 1\}^{nT \times nT}$ where the block $\tilde{\mathbf{A}}_{s,t} \in \mathbb{R}^{n \times n}$ is given by $(\mathbf{A}^{(s)} + \mathbf{A}^{(t)})/2 \in \mathbb{R}^{n \times n}$ and we denote by $\tilde{\mathbf{P}} \in [0, 1]^{nT \times nT}$ the noise-free counterpart of $\tilde{\mathbf{A}}$. If (\mathbf{z}, t) and (\mathbf{z}, t') are exchangeable, then, conditional on $\mathbf{Z}_i^{(t)} = \mathbf{Z}_i^{(t')} = \mathbf{z}$, the rows $\tilde{\mathbf{P}}_{n(t-1)+i}$ and $\tilde{\mathbf{P}}_{n(t'-1)+i}$ are equal. However, if (\mathbf{z}, t) and (\mathbf{z}', t) are exchangeable, then, in general, $\tilde{\mathbf{P}}_{n(t-1)+i} \neq \tilde{\mathbf{P}}_{n(t-1)+j}$ when $\mathbf{Z}_i^{(t)} = \mathbf{z}$ and $\mathbf{Z}_j^{(t)} = \mathbf{z}'$. One can demonstrate that two rows of $\tilde{\mathbf{P}}$ are equal if and only if the corresponding nodes’ embeddings are too. Therefore, omnibus embedding provides longitudinal but not cross-sectional stability.

Independent adjacency spectral embedding computes the spectral embeddings of the matrices $\mathbf{A}^{(t)} \in \{0, 1\}^{n \times n}$. If (\mathbf{z}, t) and (\mathbf{z}', t') are exchangeable, then, conditional on $\mathbf{Z}_i^{(t)} = \mathbf{z}$ and $\mathbf{Z}_j^{(t')} = \mathbf{z}'$, the rows $\mathbf{P}_i^{(t)}$ and $\mathbf{P}_j^{(t')}$ are equal. If $t = t'$ the embeddings of nodes i and j are equal, however, embeddings between different graphs are subject to (possibly indefinite) orthogonal transformations $\mathbf{Q}^{(t)}$ which, if $\mathbf{P}^{(t)} \neq \mathbf{P}^{(t')}$, differ in a non-trivial way (i.e. *beyond* simply reflecting the ambiguity of choosing eigenvectors in the spectral decomposition of $\mathbf{P}^{(t)}$). Therefore, independent adjacency spectral embedding provides cross-sectional but not longitudinal stability. The same arguments extend to other independent embeddings.

Separate embedding covers a collection of embedding techniques separately applied to time-averaged matrices, $\bar{\mathbf{A}}^{(t)} = \sum_k w_k \mathbf{A}^{(t-k)}$ where w_k are non-negative weights, and $\mathbf{A}^{(t)}$ may be replaced by

another matrix representation of the graph such as the normalised Laplacian. The weights may be constant, e.g. $w_k = 1/t$ for all k [40, 4], exponential forgetting factors $w_k = (1 - \lambda)^k$ [8, 19], chosen to produce a sliding window [32], based on a time series model [37], and more. In general, temporal smoothing results in two nodes behaving identically at time t being embedded differently if their past or future behaviours differ, whereas the act of embedding the matrices separately will result in the same issues of alignment encountered in independent adjacency spectral embedding. Therefore, those methods can have neither cross-sectional nor longitudinal stability, except in special cases where one can contrive to have one but not other (e.g., $w_0 = 1$ and $w_k = 0$, reducing to independent embedding). Joint embedding techniques generally aim to find an embedding to trade-off two costs: a ‘snapshot cost’ (CS) measuring the goodness-of-fit to the observed $\mathbf{A}^{(t)}$, and a ‘temporal cost’ (CT) penalising change over time. These are then combined into a single objective function, for example, as [28] (where we have replaced the normalised Laplacian by the adjacency matrix):

$$\arg \min_{\check{\mathbf{A}}^{(1)}, \dots, \check{\mathbf{A}}^{(T)}} \alpha \sum_{t=1}^T \|\mathbf{A}^{(t)} - \check{\mathbf{A}}^{(t)}\|_F^2 + (1 - \alpha) \sum_{t=1}^{T-1} \|\check{\mathbf{A}}^{(t)} - \check{\mathbf{A}}^{(t+1)}\|_F^2, \quad (11)$$

where $\alpha \in [0, 1]$, subject to a low rank constraint on $\check{\mathbf{A}}^{(1)}, \dots, \check{\mathbf{A}}^{(T)}$, where $\hat{\mathbf{Y}}^{(t)}$ is the spectral embedding of $\check{\mathbf{A}}^{(t)}$. It is easy to see that a change affecting only a fraction of the nodes will result in a change of all node embeddings, precluding both cross-sectional and longitudinal stability (again apart from contrived cases, e.g. when $\alpha = 1$).

For the complexity calculations, we assume a dense regime in which the k -truncated singular value decomposition of an m -by- n matrix is $O(kmn)$ [13]. Independent embedding is more efficient than UASE, on account of $\sum_t d_t \leq dT$, but UASE is more efficient than omnibus embedding, because of the linear versus quadratic growth in T , while $\tilde{d} = \text{rank}(\tilde{\mathbf{P}})$ is often larger than d .

5 Real data

The Lyon primary school data set shows the social interactions at a French primary school over two days in October 2009 [44]. The school consisted of 10 teachers and 241 students from five school years, each year divided into two classes. Face-to-face interactions were detected when radio-frequency identification devices worn by participants (10 teachers and 232 students gave consent to be included in the experiment) were in close proximity over an interval of 20 seconds and recorded as a pair of anonymous identifiers together with a timestamp. The data are available for download from the Network Repository website¹ [34].

A time series of networks was created by binning the data into hour-long windows over the two days, from 08:00 to 18:00 each day. If at least one interaction was observed between two people in a particular time window, an edge was created to connect the two nodes in the corresponding network. This results in a time series of graphs $\mathbf{A}^{(1)}, \dots, \mathbf{A}^{(20)}$ each with $n = 242$ nodes. Where a node is not active in a given time window, it is still included in the graph as an isolated node. This is compatible with the theory and method, and the node is embedded to the zero vector at that time point.

Given the unfolded adjacency matrix $\mathbf{A} = (\mathbf{A}^{(1)} | \dots | \mathbf{A}^{(20)})$, an estimated embedding dimension $\hat{d} = 10$ was obtained using profile likelihood [55] and we construct the embeddings $\hat{\mathbf{Y}}^{(1)}, \dots, \hat{\mathbf{Y}}^{(20)} \in \mathbb{R}^{n \times 10}$, taking approximately five seconds on a 2017 MacBook Pro. Figure 2 shows the first two dimensions of this embedding to visualise some of the structure in the data. Similar plots and discussion for both individual spectral embedding and omnibus embedding are given in the Appendix.

From this plot, we observe clustering of students in the same school class. For time windows corresponding to classroom time, for example, 09:00–10:00 and 15:00–16:00, the embedding forms rays of points in 10-dimensional space, with each ray broadly corresponding to a single school class. This is to be expected under a degree-corrected stochastic block model, and the distance along the ray is a measure of the node’s activity level [25, 30, 38]. However, not all time windows exhibit this structure, for example, the different classes mix more during lunchtimes (time windows 12:00–13:00 and 13:00–14:00).

¹<https://networkrepository.com>

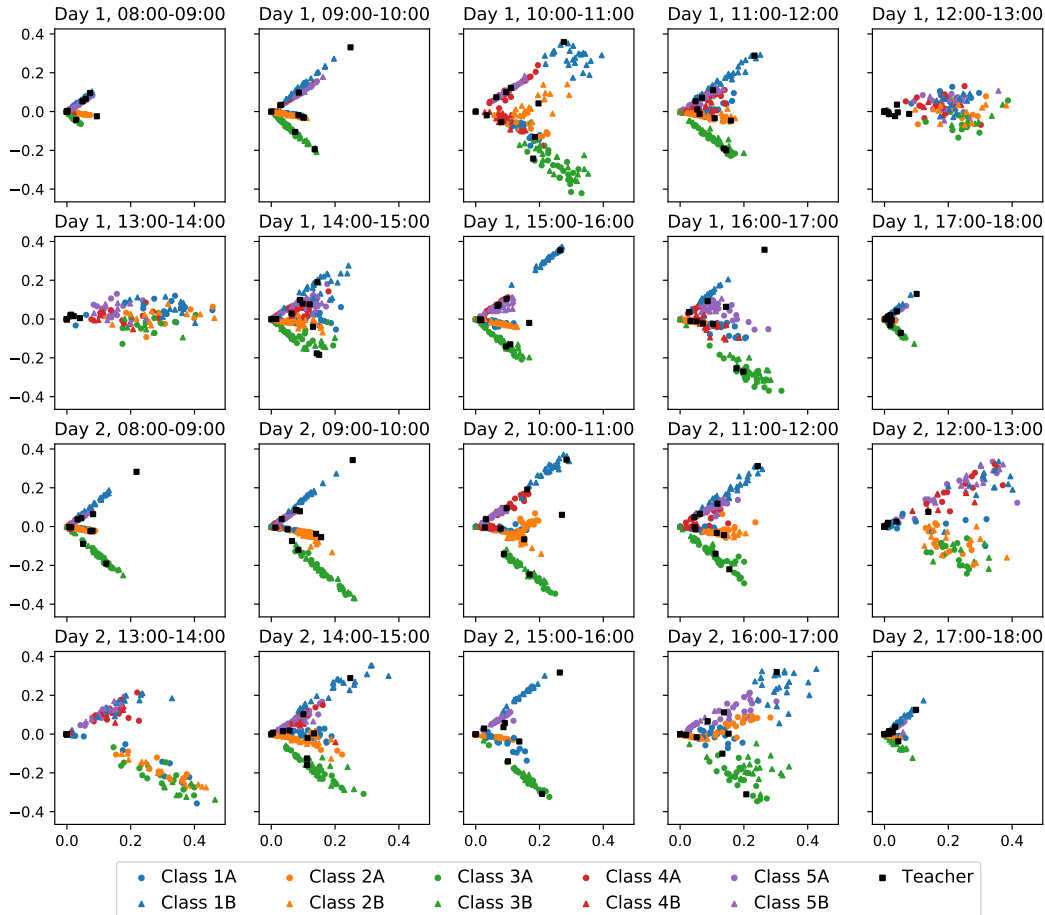


Figure 2: First two dimensions of the embeddings $\hat{\mathbf{Y}}^{(1)}, \dots, \hat{\mathbf{Y}}^{(20)}$ of the unfolded adjacency matrix $\mathbf{A} = (\mathbf{A}^{(1)} | \dots | \mathbf{A}^{(20)})$. The colours indicate different school years while the marker type distinguishes the two school classes within each year.

5.1 Clustering

Following recommendations regarding community detection under a degree-corrected stochastic block model [38], we analyse UASE using spherical coordinates $\Theta^{(t)} \in [0, 2\pi)^{n \times 9}$, for $t \in [T]$. Since UASE demonstrates cross-sectional and longitudinal stability, we can combine the embeddings into a single point cloud $\Theta = (\Theta^{(1)\top} | \dots | \Theta^{(T)\top})^\top \in \mathbb{R}^{nT \times 9}$ where each point represents a student or teacher in a particular time window. This allows us to detect people returning to a previous behaviour in the dynamic network. We fit a Gaussian mixture model with varying covariance matrices to the non-zero points in Θ with 20–50 clusters increasing in increments of 5, with 50 random initialisations, taking approximately five minutes on a 2017 MacBook Pro. Using the Bayesian Information Criterion, we select the best fitting model (30 clusters) and assign the maximum a posteriori Gaussian cluster membership to each student in each time window.

Figure 3 shows how students in the ten classes move between these clusters over time. Each class has one or two clusters unique to it, for example, the majority of students in class 1A spend their classroom time (as opposed to break time) assigned to cluster 1 or cluster 25. This highlights the importance of longitudinal stability in UASE, as we are detecting points in the embedding returning to some part of latent space.

There are also instances of multiple school classes being assigned the same cluster at the same time period, for example, on the morning of day 1, classes 5A and 5B are mainly in cluster 28 suggesting

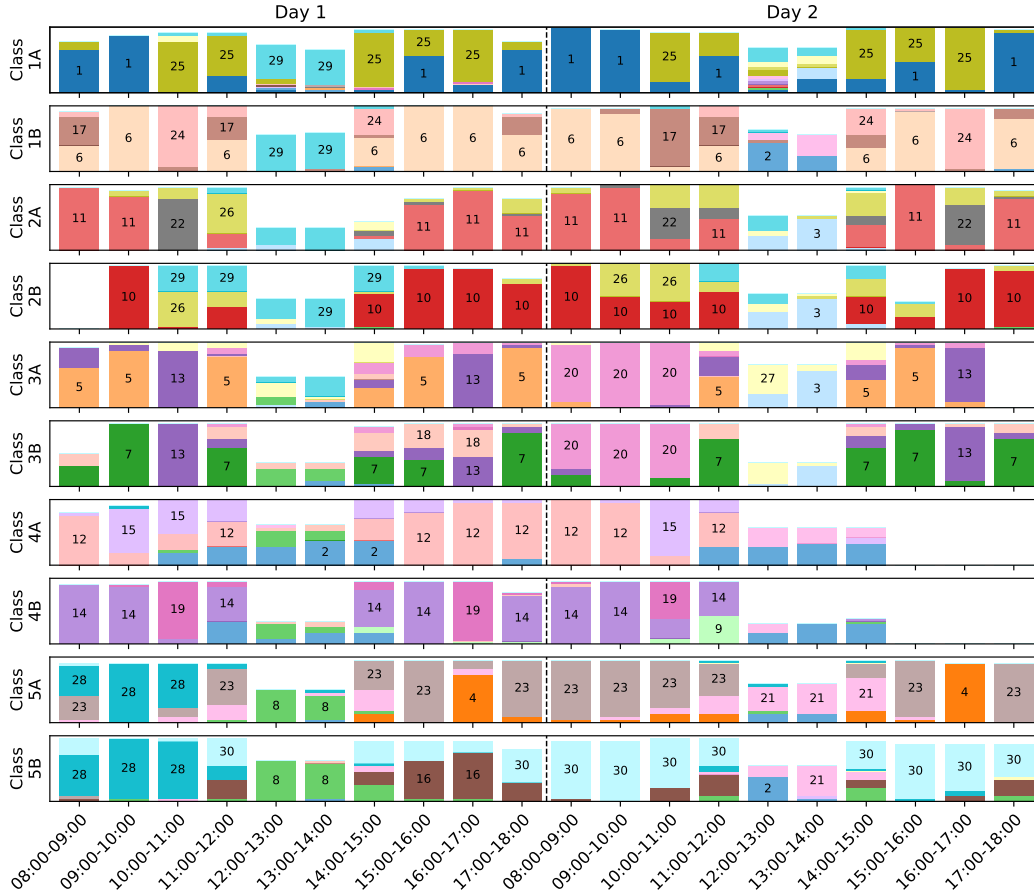


Figure 3: Bar chart showing the Gaussian cluster assignment of school classes over time. The height of each coloured bar represents the proportion of students, in that class and at that time, assigned to the corresponding Gaussian cluster, the total available height representing 100%. If the coloured bars do not sum to the full available height, the difference represents the proportion of inactive students. For legibility, only bars representing over 35% of the class are labelled with the cluster number.

they are having a joint lesson, and we see this behaviour again on day 2 with classes 3A and 3B in cluster 20. In the lunchtime periods, particularly on day 1, the younger students (classes 1A–2B) mingle to form a larger cluster, as do the older students (classes 4A–5B), potentially explained by the cafeteria needing two sittings for lunch for space reasons [44]. This highlights the importance of cross-sectional stability in UASE, as it allows the grouping of nodes behaving similarly in a specific time window, irrespective of their potentially different past and future behaviours.

6 Conclusion

We prove that an existing procedure, UASE, allows dynamic network embedding with longitudinal and cross-sectional stability guarantees. These properties make a range of subsequent spatio-temporal analyses possible using ‘off-the-shelf’ techniques for clustering, time series analysis, classification and more.

Funding Transparency Statement

Andrew Jones and Patrick Rubin-Delanchy’s research was supported by an Alan Turing Institute fellowship. Ian Gallagher’s research was supported by an EPSRC PhD studentship.

References

- [1] Abbe, E. (2017). Community detection and stochastic block models: recent developments. *The Journal of Machine Learning Research*, 18(1):6446–6531.
- [2] Agterberg, J., Tang, M., and Priebe, C. E. (2020). On two distinct sources of nonidentifiability in latent position random graph models. *arXiv preprint arXiv:2003.14250*.
- [3] Amini, A. A., Chen, A., Bickel, P. J., and Levina, E. (2013). Pseudo-likelihood methods for community detection in large sparse networks. *The Annals of Statistics*, 41(4):2097–2122.
- [4] Bhattacharyya, S. and Chatterjee, S. (2018). Spectral clustering for multiple sparse networks: I. *arXiv preprint arXiv:1805.10594*.
- [5] Chen, H. and Li, J. (2018). Exploiting structural and temporal evolution in dynamic link prediction. In *Proceedings of the 27th ACM International Conference on Information and Knowledge Management*, pages 427–436.
- [6] Chi, Y., Song, X., Zhou, D., Hino, K., and Tseng, B. L. (2007). Evolutionary spectral clustering by incorporating temporal smoothness. In *Proceedings of the 13th ACM SIGKDD international conference on Knowledge discovery and data mining*, pages 153–162.
- [7] Deng, D., Shahabi, C., Demiryurek, U., Zhu, L., Yu, R., and Liu, Y. (2016). Latent space model for road networks to predict time-varying traffic. In *Proceedings of the 22nd ACM SIGKDD International Conference on Knowledge Discovery and Data Mining*, pages 1525–1534.
- [8] Dunlavy, D. M., Kolda, T. G., and Acar, E. (2011). Temporal link prediction using matrix and tensor factorizations. *ACM Transactions on Knowledge Discovery from Data (TKDD)*, 5(2):1–27.
- [9] Durante, D. and Dunson, D. B. (2014). Nonparametric Bayes dynamic modelling of relational data. *Biometrika*, 101(4):883–898.
- [10] Durante, D., Mukherjee, N., and Steorts, R. C. (2017). Bayesian learning of dynamic multilayer networks. *The Journal of Machine Learning Research*, 18(1):1414–1442.
- [11] Friel, N., Rastelli, R., Wyse, J., and Raftery, A. E. (2016). Interlocking directorates in Irish companies using a latent space model for bipartite networks. *Proceedings of the National Academy of Sciences*, 113(24):6629–6634.
- [12] Gao, S., Denoyer, L., and Gallinari, P. (2011). Temporal link prediction by integrating content and structure information. In *Proceedings of the 20th ACM international conference on Information and knowledge management*, pages 1169–1174.
- [13] Gu, M. and Eisenstat, S. C. (1996). Efficient algorithms for computing a strong rank-revealing qr factorization. *SIAM Journal on Scientific Computing*, 17(4):848–869.
- [14] Ho, Q., Song, L., and Xing, E. (2011). Evolving cluster mixed-membership blockmodel for time-evolving networks. In *Proceedings of the Fourteenth International Conference on Artificial Intelligence and Statistics*, pages 342–350. JMLR Workshop and Conference Proceedings.
- [15] Hoff, P. D. (2011). Hierarchical multilinear models for multiway data. *Computational Statistics & Data Analysis*, 55(1):530–543.
- [16] Hoff, P. D. et al. (2011). Separable covariance arrays via the Tucker product, with applications to multivariate relational data. *Bayesian Analysis*, 6(2):179–196.
- [17] Jones, A. and Rubin-Delanchy, P. (2021). The multilayer random dot product graph. *arXiv preprint arXiv:2007.10455*.
- [18] Karrer, B. and Newman, M. E. J. (2011). Stochastic blockmodels and community structure in networks. *Phys. Rev. E (3)*, 83(1):016107, 10.
- [19] Keriven, N. and Vaiter, S. (2020). Sparse and smooth: improved guarantees for spectral clustering in the dynamic stochastic block model. *arXiv preprint arXiv:2002.02892*.

- [20] Kim, B., Lee, K. H., Xue, L., and Niu, X. (2018). A review of dynamic network models with latent variables. *Statistics surveys*, 12:105.
- [21] Krzakala, F., Moore, C., Mossel, E., Neeman, J., Sly, A., Zdeborová, L., and Zhang, P. (2013). Spectral redemption in clustering sparse networks. *Proceedings of the National Academy of Sciences*, 110(52):20935–20940.
- [22] Lee, N. H. and Priebe, C. E. (2011). A latent process model for time series of attributed random graphs. *Statistical inference for stochastic processes*, 14(3):231–253.
- [23] Lee, N. H., Yoder, J., Tang, M., and Priebe, C. E. (2013). On latent position inference from doubly stochastic messaging activities. *Multiscale Modeling & Simulation*, 11(3):683–718.
- [24] Lei, J. (2021). Network representation using graph root distributions. *The Annals of Statistics*, 49(2):745–768.
- [25] Lei, J. and Rinaldo, A. (2015). Consistency of spectral clustering in stochastic block models. *Ann. Statist.*, 43(1):215–237.
- [26] Levin, K., Athreya, A., Tang, M., Lyzinski, V., Park, Y., and Priebe, C. E. (2017). A central limit theorem for an omnibus embedding of multiple random graphs and implications for multiscale network inference. *arXiv preprint arXiv:1705.09355*.
- [27] Lin, Y.-R., Chi, Y., Zhu, S., Sundaram, H., and Tseng, B. L. (2008). Facetnet: a framework for analyzing communities and their evolutions in dynamic networks. In *Proceedings of the 17th international conference on World Wide Web*, pages 685–694.
- [28] Liu, F., Choi, D., Xie, L., and Roeder, K. (2018). Global spectral clustering in dynamic networks. *Proceedings of the National Academy of Sciences*, 115(5):927–932.
- [29] Liu, S., Wang, S., and Krishnan, R. (2014). Persistent community detection in dynamic social networks. In *Pacific-Asia Conference on Knowledge Discovery and Data Mining*, pages 78–89. Springer.
- [30] Lyzinski, V., Sussman, D. L., Tang, M., Athreya, A., and Priebe, C. E. (2014). Perfect clustering for stochastic blockmodel graphs via adjacency spectral embedding. *Electron. J. Stat.*, 8(2):2905–2922.
- [31] Matias, C. and Miele, V. (2015). Statistical clustering of temporal networks through a dynamic stochastic block model. *arXiv preprint arXiv:1506.07464*.
- [32] Pensky, M., Zhang, T., et al. (2019). Spectral clustering in the dynamic stochastic block model. *Electronic Journal of Statistics*, 13(1):678–709.
- [33] Robinson, L. F. and Priebe, C. E. (2012). Detecting time-dependent structure in network data via a new class of latent process models. *arXiv preprint arXiv:1212.3587*.
- [34] Rossi, R. A. and Ahmed, N. K. (2015). The network data repository with interactive graph analytics and visualization. In *AAAI*.
- [35] Rubin-Delanchy, P. (2020). Manifold structure in graph embeddings. In *Proceedings of the Thirty-fourth Conference on Neural Information Processing Systems*.
- [36] Rubin-Delanchy, P., Cape, J., Priebe, C. E., and Tang, M. (2020). A statistical interpretation of spectral embedding: the generalised random dot product graph. *arXiv preprint arXiv:1709.05506v3*.
- [37] Sanna Passino, F., Bertiger, A. S., Neil, J. C., and Heard, N. A. (2019). Link prediction in dynamic networks using random dot product graphs. *arXiv preprint arXiv:1912.10419*.
- [38] Sanna Passino, F., Heard, N. A., and Rubin-Delanchy, P. (2020). Spectral clustering on spherical coordinates under the degree-corrected stochastic blockmodel. *arXiv e-prints*, pages arXiv–2011.
- [39] Sarkar, P. and Moore, A. W. (2005). Dynamic social network analysis using latent space models. *ACM SigKDD Explorations Newsletter*, 7(2):31–40.

- [40] Scheinerman, E. R. and Tucker, K. (2010). Modeling graphs using dot product representations. *Computational statistics*, 25(1):1–16.
- [41] Seshadhri, C., Sharma, A., Stolman, A., and Goel, A. (2020). The impossibility of low-rank representations for triangle-rich complex networks. *Proceedings of the National Academy of Sciences*, 117(11):5631–5637.
- [42] Seto, S., Zhang, W., and Zhou, Y. (2015). Multivariate time series classification using dynamic time warping template selection for human activity recognition. In *2015 IEEE Symposium Series on Computational Intelligence*, pages 1399–1406. IEEE.
- [43] Sewell, D. K. and Chen, Y. (2015). Latent space models for dynamic networks. *Journal of the American Statistical Association*, 110(512):1646–1657.
- [44] Stehlé, J., Voirin, N., Barrat, A., Cattuto, C., Isella, L., Pinton, J.-F., Quaghiotto, M., Van den Broeck, W., Régis, C., Lina, B., et al. (2011). High-resolution measurements of face-to-face contact patterns in a primary school. *PloS one*, 6(8):e23176.
- [45] Turnbull, K. (2020). *Advancements in latent space network modelling*. PhD thesis, Lancaster University.
- [46] Udell, M. and Townsend, A. (2019). Why are big data matrices approximately low rank? *SIAM Journal on Mathematics of Data Science*, 1(1):144–160.
- [47] Xie, Y., Li, C., Yu, B., Zhang, C., and Tang, Z. (2020). A survey on dynamic network embedding. *arXiv preprint arXiv:2006.08093*.
- [48] Xing, E. P., Fu, W., Song, L., et al. (2010). A state-space mixed membership blockmodel for dynamic network tomography. *Annals of Applied Statistics*, 4(2):535–566.
- [49] Xu, K. (2015). Stochastic block transition models for dynamic networks. In *Artificial Intelligence and Statistics*, pages 1079–1087. PMLR.
- [50] Xu, K. S. and Hero, A. O. (2014). Dynamic stochastic blockmodels for time-evolving social networks. *IEEE Journal of Selected Topics in Signal Processing*, 8(4):552–562.
- [51] Xue, G., Zhong, M., Li, J., Chen, J., Zhai, C., and Kong, R. (2021). Dynamic network embedding survey. *arXiv preprint arXiv:2103.15447*.
- [52] Yang, T., Chi, Y., Zhu, S., Gong, Y., and Jin, R. (2011). Detecting communities and their evolutions in dynamic social networks—a Bayesian approach. *Machine learning*, 82(2):157–189.
- [53] Zhao, B., Lu, H., Chen, S., Liu, J., and Wu, D. (2017). Convolutional neural networks for time series classification. *Journal of Systems Engineering and Electronics*, 28(1):162–169.
- [54] Zhu, L., Guo, D., Yin, J., Ver Steeg, G., and Galstyan, A. (2016). Scalable temporal latent space inference for link prediction in dynamic social networks. *IEEE Transactions on Knowledge and Data Engineering*, 28(10):2765–2777.
- [55] Zhu, M. and Ghodsi, A. (2006). Automatic dimensionality selection from the scree plot via the use of profile likelihood. *Computational Statistics & Data Analysis*, 51(2):918–930.

A Appendix

Python notebooks producing the figures of this paper are available at <https://github.com/iggallagher/Dynamic-Network-Embedding>.

Proof of Theorem 1

Given the factorisation

$$f(\mathbf{x}, \mathbf{y}) = \sum_{i=1}^D \lambda_i u_i(\mathbf{x}) u_i(\mathbf{y}), \quad (12)$$

define a map $\phi : \mathcal{Z} \rightarrow \mathbb{R}^D$ by setting the i th coordinate of $\phi(\mathbf{z})$ to be $|\lambda_i|^{1/2} u_i(\mathbf{z})$, so that for any $\mathbf{x}, \mathbf{y} \in \mathcal{Z}$ we have $f(\mathbf{x}, \mathbf{y}) = \phi(\mathbf{x})^\top \mathbf{I}_{p,q} \phi(\mathbf{y})$ (where $\mathbf{I}_{p,q}$ is the diagonal matrix whose entries are the signs of the eigenvalues λ_i). Let \mathcal{F}^* be the joint distribution on \mathbb{R}^{TD} obtained by first assigning a random vector $\zeta = (\zeta_1 | \dots | \zeta_T)$ via \mathcal{F} and then applying the map ϕ to each of the components ζ_t , and let $\mathcal{F}_1^*, \dots, \mathcal{F}_T^*$ denote the corresponding marginal distributions on \mathbb{R}^D . Given $\xi \sim \mathcal{F}^*$ and $\xi_t \sim \mathcal{F}_t^*$, define the second moment matrices $\Delta = \mathbb{E}[\xi \xi^\top] \in \mathbb{R}^{TD \times TD}$ and $\Delta_t = \mathbb{E}[\xi_t \xi_t^\top] \in \mathbb{R}^{D \times D}$, and let $r = \text{rank}(\Delta)$ and $r_t = \text{rank}(\Delta_t)$.

Let $\mathbf{M} \in \mathbb{R}^{r \times TD}$ be a matrix whose rows form a basis of $\text{supp}(\mathcal{F}^*)$, and similarly let $\mathbf{N}_t \in \mathbb{R}^{r_t \times D}$ be a matrix whose rows form a basis of $\text{supp}(\mathcal{F}_t^*)$. Let $\mathbf{N} = \text{diag}(\mathbf{N}_1, \dots, \mathbf{N}_T)$, and define the matrix $\mathbf{\Pi} := \mathbf{M} \mathbf{D} \mathbf{N}^\top \in \mathbb{R}^{r \times (r_1 + \dots + r_T)}$, where $\mathbf{D} = \text{diag}(\mathbf{I}_{p,q}, \dots, \mathbf{I}_{p,q})$. Construct the singular value decomposition $\mathbf{\Pi} = \mathbf{U} \mathbf{\Sigma} \mathbf{V}^\top$, with $\mathbf{U} \in O(r \times d)$, $\mathbf{\Sigma} \in \mathbb{R}^{d \times d}$ and $\mathbf{V} \in O((r_1 + \dots + r_T) \times d)$, and $d = \text{rank}(\mathbf{\Pi})$. Writing $\mathbf{V} = (\mathbf{V}_1 | \dots | \mathbf{V}_T)$, where $\mathbf{V}_t \in \mathbb{R}^{r_t \times d}$ has rank d_r , we can then construct the singular value decompositions $\mathbf{V}_t = \mathbf{U}_t \mathbf{\Sigma}_t \mathbf{W}_t^\top$, with $\mathbf{U}_t \in O(r_t \times d_t)$, $\mathbf{\Sigma}_t \in \mathbb{R}^{d_t \times d_t}$ and $\mathbf{W}_t \in O(d \times d_t)$, where $d_t = \text{rank}(\mathbf{V}_t)$.

Define $\mathbf{\Lambda} = \mathbf{\Sigma} \mathbf{W} \in \mathbb{R}^{d \times (d_1 + \dots + d_T)}$, where $\mathbf{W} = (\mathbf{W}_1 \mathbf{\Sigma}_1 | \dots | \mathbf{W}_T \mathbf{\Sigma}_T)$, and let $L : \mathbb{R}^{TD} \rightarrow \mathbb{R}^d$ be the linear map sending the i th row of \mathbf{M} to the i th row of \mathbf{U} , and similarly let $L_t : \mathbb{R}^D \rightarrow \mathbb{R}^{d_t}$ be the linear map sending the i th row of \mathbf{N}_t to the i th row of \mathbf{U}_t . Finally, let $\varphi : \mathbb{R}^{T^k} \rightarrow \mathbb{R}^d$ and $\varphi_t : \mathbb{R}^k \rightarrow \mathbb{R}^{d_t}$ be the maps satisfying $\varphi(\mathbf{z}) = L((\phi(\mathbf{z}^{(1)}) | \dots | \phi(\mathbf{z}^{(T)})))$ and $\varphi_t(\mathbf{z}^{(t)}) = L_t(\phi(\mathbf{z}^{(t)}))$ for any $\mathbf{z} = (\mathbf{z}^{(1)} | \dots | \mathbf{z}^{(T)}) \in \mathbb{R}^{T^k}$.

Then, setting \mathcal{G} to be the joint distribution on $\mathbb{R}^d \times \mathbb{R}^{d_1} \times \dots \times \mathbb{R}^{d_T}$ obtained by first assigning a random vector $\zeta = (\zeta_1 | \dots | \zeta_T)$ via \mathcal{F} and then sending this to the tuple $(\varphi(\zeta), \varphi_1(\zeta_1), \dots, \varphi_T(\zeta_T))$ and letting $\mathbf{X}_i = \varphi(\mathbf{Z}_i)$ and $\mathbf{Y}_i^{(t)} = \varphi_t(\mathbf{Z}_i^{(t)})$, we find that $(\mathbf{A}, \mathbf{X}, \mathbf{Y}) \sim \text{MRDPG}(\mathcal{G}, \mathbf{\Lambda})$. \square

Proof of Proposition 2

This follows directly from Theorem 1 in [17], which states that there exist sequences of matrices $\mathbf{R}_t = \mathbf{R}_t(n) \in \mathbb{R}^{d_t \times d}$ and $\tilde{\mathbf{W}} \in O(d)$ such that

$$\|\hat{\mathbf{Y}}^{(t)} - \mathbf{Y}^{(t)} \mathbf{R}_t \tilde{\mathbf{W}}^\top\|_{2 \rightarrow \infty} = O\left(\frac{\log^{1/2}(n)}{\rho^{1/2} n^{1/2}}\right) \quad (13)$$

almost surely, where the matrices \mathbf{R}_t satisfy $\tilde{\mathbf{Y}}^{(t)} = \mathbf{Y}^{(t)} \mathbf{R}_{\mathbf{Y},t}$, and $\tilde{\mathbf{W}} \in O(d)$ is the solution to the one-mode orthogonal Procrustes problem

$$\tilde{\mathbf{W}} = \arg \min_{\mathbf{Q} \in O(d)} \|\mathbf{U}_A \mathbf{Q} - \mathbf{U}_P\|_F^2 + \|\mathbf{V}_A \mathbf{Q} - \mathbf{V}_P\|_F^2, \quad (14)$$

where \mathbf{A} and \mathbf{P} admit the singular value decompositions $\mathbf{A} = \mathbf{U}_A \mathbf{\Sigma}_A \mathbf{V}_A^\top + \mathbf{U}_{A,\perp} \mathbf{\Sigma}_{A,\perp} \mathbf{V}_{A,\perp}^\top$ and $\mathbf{P} = \mathbf{U}_P \mathbf{\Sigma}_P \mathbf{V}_P^\top$ respectively. Observing that the 2-to-infinity norm of a matrix is known to be equivalent to its maximum Euclidean row norm (and consequently is invariant under orthogonal transformations) gives the desired result. \square

Proof of Proposition 3

From the proof of Theorem 1 in [17], we find that

$$n^{1/2}(\hat{\mathbf{Y}}^{(t)} \tilde{\mathbf{W}} - \tilde{\mathbf{Y}}^{(t)}) = n^{1/2}(\mathbf{A}^{(t)} - \mathbf{P}^{(t)}) \mathbf{U}_P \mathbf{\Sigma}_P^{-1/2} + n^{1/2} \mathbf{E}, \quad (15)$$

where the residual term \mathbf{E} satisfies $\|n^{1/2}\mathbf{E}\|_{2 \rightarrow \infty} \rightarrow 0$. We can rewrite this as

$$n^{1/2}(\hat{\mathbf{Y}}^{(t)}\tilde{\mathbf{W}} - \tilde{\mathbf{Y}}^{(t)}) = n^{1/2}(\mathbf{A}^{(t)} - \mathbf{P}^{(t)})\mathbf{X}\mathbf{L}\Sigma_{\mathbf{P}}^{-1} + n^{1/2}\mathbf{E}, \quad (16)$$

where $\mathbf{L} \in \text{GL}(d)$ (the general linear group of invertible $d \times d$ matrices) satisfies $\mathbf{X} = \tilde{\mathbf{X}}\mathbf{L}$, which is known to exist by Proposition 16 of [17].

We begin by showing that there exists a sequence of orthogonal matrices $\mathbf{W} \in O(d)$ and a fixed matrix $\tilde{\mathbf{L}} \in \mathbb{R}^{d \times d}$ such that $\mathbf{L}\mathbf{W}_* \rightarrow \tilde{\mathbf{L}}$, for which we adapt the arguments of Theorem 1 and Corollary 2 of [2].

To begin with, note that the mapping $v \mapsto \mathbf{X}(\mathbf{X}^\top\mathbf{X})^{-1/2}v$ sends the eigenvectors of the matrix $(\mathbf{X}^\top\mathbf{X})^{1/2}\mathbf{\Lambda}\mathbf{Y}^\top\mathbf{Y}\mathbf{\Lambda}^\top(\mathbf{X}^\top\mathbf{X})^{1/2}$ to the left singular vectors of \mathbf{P} , since if v is such an eigenvector (with corresponding eigenvalue λ) then

$$\mathbf{P}\mathbf{P}^\top\mathbf{X}(\mathbf{X}^\top\mathbf{X})^{-1/2}v = \mathbf{X}\mathbf{\Lambda}\mathbf{Y}^\top\mathbf{Y}\mathbf{\Lambda}^\top(\mathbf{X}^\top\mathbf{X})^{1/2}v \quad (17)$$

$$= \mathbf{X}(\mathbf{X}^\top\mathbf{X})^{-1/2}(\mathbf{X}^\top\mathbf{X})^{1/2}\mathbf{\Lambda}\mathbf{Y}^\top\mathbf{Y}\mathbf{\Lambda}^\top(\mathbf{X}^\top\mathbf{X})^{1/2}v \quad (18)$$

$$= \lambda\mathbf{X}(\mathbf{X}^\top\mathbf{X})^{-1/2}v \quad (19)$$

as required. Thus we may write $\mathbf{U}_{\mathbf{P}} = \mathbf{X}(\mathbf{X}^\top\mathbf{X})^{-1/2}\mathbf{V}$, where \mathbf{V} is a matrix of eigenvectors of $(\mathbf{X}^\top\mathbf{X})^{1/2}\mathbf{\Lambda}\mathbf{Y}^\top\mathbf{Y}\mathbf{\Lambda}^\top(\mathbf{X}^\top\mathbf{X})^{1/2}$, and consequently observe that

$$\mathbf{L} = (\mathbf{X}^\top\mathbf{X})^{-1}\mathbf{X}^\top\mathbf{X}_{\mathbf{P}} \quad (20)$$

$$= (\mathbf{X}^\top\mathbf{X})^{-1}\mathbf{X}^\top\mathbf{X}(\mathbf{X}^\top\mathbf{X})^{-1/2}\mathbf{V}\Sigma_{\mathbf{P}}^{1/2} \quad (21)$$

$$= (\mathbf{X}^\top\mathbf{X})^{-1/2}\mathbf{V}\Sigma_{\mathbf{P}}^{1/2} \quad (22)$$

$$= \left(\frac{\mathbf{X}^\top\mathbf{X}}{n}\right)^{-1/2}\mathbf{V}\left(\frac{\Sigma_{\mathbf{P}}}{n}\right)^{1/2}. \quad (23)$$

Let $\mathcal{G}_{\mathbf{X}}$ and $\mathcal{G}_{\mathbf{Y},t}$ denote the marginal distributions of \mathcal{G} , and define the second moment matrices $\Delta_{\mathbf{X}} = \mathbb{E}[\xi\xi^\top]$ and $\Delta_{\mathbf{Y},t} = \mathbb{E}[\xi_t\xi_t^\top]$, where $\xi \sim \mathcal{G}_{\mathbf{X}}$ and $\xi_t \sim \mathcal{G}_{\mathbf{Y},t}$, and let $\Delta_{\mathbf{Y}} = \text{diag}(\Delta_{\mathbf{Y},1}, \dots, \Delta_{\mathbf{Y},T})$. Then the law of large numbers tells us that the first and last terms in (23) converge to $(\rho_n\Delta_{\mathbf{X}})^{-1/2}$ and $(\rho_n\tilde{\Sigma})^{1/2}$ respectively, where $\tilde{\Sigma}$ is the diagonal matrix whose entries are the square roots of the eigenvalues of $\Delta_{\mathbf{X}}^{1/2}\mathbf{\Lambda}\Delta_{\mathbf{Y}}\mathbf{\Lambda}^\top\Delta_{\mathbf{X}}^{1/2}$ (see, for example, Proposition 7 of [17]). Note that \mathbf{V} is also the matrix of eigenvectors of

$$\left(\frac{\mathbf{X}^\top\mathbf{X}}{n}\right)^{1/2}\left(\frac{\mathbf{\Lambda}\mathbf{Y}^\top\mathbf{Y}\mathbf{\Lambda}^\top}{n}\right)\left(\frac{\mathbf{X}^\top\mathbf{X}}{n}\right)^{1/2} \quad (24)$$

which converges to $\Delta_{\mathbf{X}}^{1/2}\mathbf{\Lambda}\Delta_{\mathbf{Y}}\mathbf{\Lambda}^\top\Delta_{\mathbf{X}}^{1/2}$ by the law of large numbers. Consequently, for each distinct eigenvalue of $\Delta_{\mathbf{X}}^{1/2}\mathbf{\Lambda}\Delta_{\mathbf{Y}}\mathbf{\Lambda}^\top\Delta_{\mathbf{X}}^{1/2}$ we may apply the Davis-Kahan theorem to find that the principal angles between the resulting eigenspace and the subspace spanned by the corresponding columns of \mathbf{V} vanish, and thus \mathbf{V} converges to $\tilde{\mathbf{V}}$ up to some block-orthogonal transformation $\mathbf{W} \in O(d)$, where $\tilde{\mathbf{V}}$ is a fixed matrix of eigenvectors of $\Delta_{\mathbf{X}}^{1/2}\mathbf{\Lambda}\Delta_{\mathbf{Y}}\mathbf{\Lambda}^\top\Delta_{\mathbf{X}}^{1/2}$. Since \mathbf{W} by definition commutes with $\tilde{\Sigma}$, we find that

$$\mathbf{L}\mathbf{W} \rightarrow \Delta_{\mathbf{X}}^{-1/2}\tilde{\mathbf{V}}\tilde{\Sigma}^{1/2} \quad (25)$$

as required.

Multiplying (16) by \mathbf{W} , we find that

$$n^{1/2}(\hat{\mathbf{Y}}_i^{(t)}\tilde{\mathbf{W}} - \tilde{\mathbf{Y}}_i^{(t)})\mathbf{W} \approx n\rho_n \left[\frac{1}{n^{1/2}\rho_n}(\mathbf{A}^{(t)} - \mathbf{P}^{(t)})\mathbf{X} \right]_i \mathbf{L}\Sigma_{\mathbf{P}}^{-1}\mathbf{W} \quad (26)$$

and note that the term $n\rho_n\mathbf{L}\Sigma_{\mathbf{P}}^{-1}\mathbf{W}$ converges to $\tilde{\mathbf{L}}\tilde{\Sigma}^{-1}$ from our previous discussion. Moreover,

$$\left[\frac{1}{n^{1/2}\rho_n}(\mathbf{A}^{(t)} - \mathbf{P}^{(t)})\mathbf{X} \right]_i = \frac{1}{n^{1/2}\rho_n} \sum_{j=1}^n (\mathbf{A}_{ij}^{(t)} - \mathbf{P}_{ij}^{(t)})\mathbf{X}_j \quad (27)$$

$$= \frac{1}{(n\rho_n)^{1/2}} \sum_{j=1}^n (\mathbf{A}_{ij}^{(t)} - \mathbf{P}_{ij}^{(t)})\varphi(\mathbf{Z}_j). \quad (28)$$

Conditional on $\mathbf{Z}_i^{(t)} = \mathbf{z}$, we have $\mathbf{P}_{ij}^{(t)} = \rho_n f(\mathbf{z}, \mathbf{Z}_j^{(t)})$, and so the sum in (28) is a scaled sum of $n - 1$ independent, identically distributed zero-mean random variables, each with covariance matrix

$$\mathbb{E}_\zeta \left[f(\mathbf{z}, \zeta_t) (1 - \rho_n f(\mathbf{z}, \zeta_t)) \cdot \varphi(\zeta)^\top \varphi(\zeta) \right] \quad (29)$$

where $\zeta \sim \mathcal{F}$, from which the result follows by setting $\mathbf{R}_* = \tilde{\Sigma}^{-1} \tilde{\mathbf{L}}^\top$ and applying the multivariate versions of the central limit theorem and Slutsky's theorem. \square

Proof of Corollary 5

Note that for any $t \in [T]$ the equality $\tilde{\mathbf{X}} \tilde{\mathbf{Y}}^{(t)\top} = \mathbf{P}^{(t)}$ holds, and so $\tilde{\mathbf{Y}}^{(t)} = \mathbf{P}^{(t)} \tilde{\mathbf{X}} (\tilde{\mathbf{X}}^\top \tilde{\mathbf{X}})^{-1}$ (since $\mathbf{P}^{(t)}$ is symmetric). Consequently, for any $i \in [n]$ we find that $\tilde{\mathbf{Y}}_i^{(t)} = (\tilde{\mathbf{X}}^\top \tilde{\mathbf{X}})^{-1} \tilde{\mathbf{X}}^\top \mathbf{P}_i^{(t)}$, where $\mathbf{P}_i^{(t)}$ denotes the i th row of $\mathbf{P}^{(t)}$ (again due to symmetry of $\mathbf{P}^{(t)}$). Thus for any exchangeable pair (\mathbf{z}, t) and (\mathbf{z}', t') , if $\mathbf{Z}_i^{(t)} = \mathbf{z}$ and $\mathbf{Z}_j^{(t')} = \mathbf{z}'$ then the equality of the rows $\mathbf{P}_i^{(t)}$ and $\mathbf{P}_j^{(t')}$ implies the equality of $\tilde{\mathbf{Y}}_i^{(t)}$ and $\tilde{\mathbf{Y}}_j^{(t')}$. Moreover, from the definition of exchangeability it is clear that the matrices $\Sigma_t(\mathbf{z})$ and $\Sigma_{t'}(\mathbf{z}')$ present in the limiting distributions for $\hat{\mathbf{Y}}_i^{(t)}$ and $\hat{\mathbf{Y}}_j^{(t')}$ in Proposition 3 are equal, and since the matrices \mathbf{W} , $\tilde{\mathbf{W}}$ and \mathbf{R}_* are independent of t and t' equality of the full covariance matrices follows.

An analogous argument holds in the case that (\mathbf{z}, t) and (\mathbf{z}', t') are exchangeable up to degree. \square

Lyon primary school data: other embeddings

In this section, we show the spectral embeddings for the Lyon primary school data for two other embedding algorithms: independent adjacency spectral embedding and omnibus embedding.

First, for the adjacency matrices $\mathbf{A}^{(1)}, \dots, \mathbf{A}^{(20)}$, we construct the adjacency spectral embeddings $\hat{\mathbf{Y}}^{(1)}, \dots, \hat{\mathbf{Y}}^{(20)} \in \mathbb{R}^{n \times 10}$, using the same dimension as the equivalent UASE for this data. This takes approximately 0.2 seconds on a 2017 MacBook Pro. Figure 4 shows the first two dimensions of this embedding to visualise some of the structure in the data.

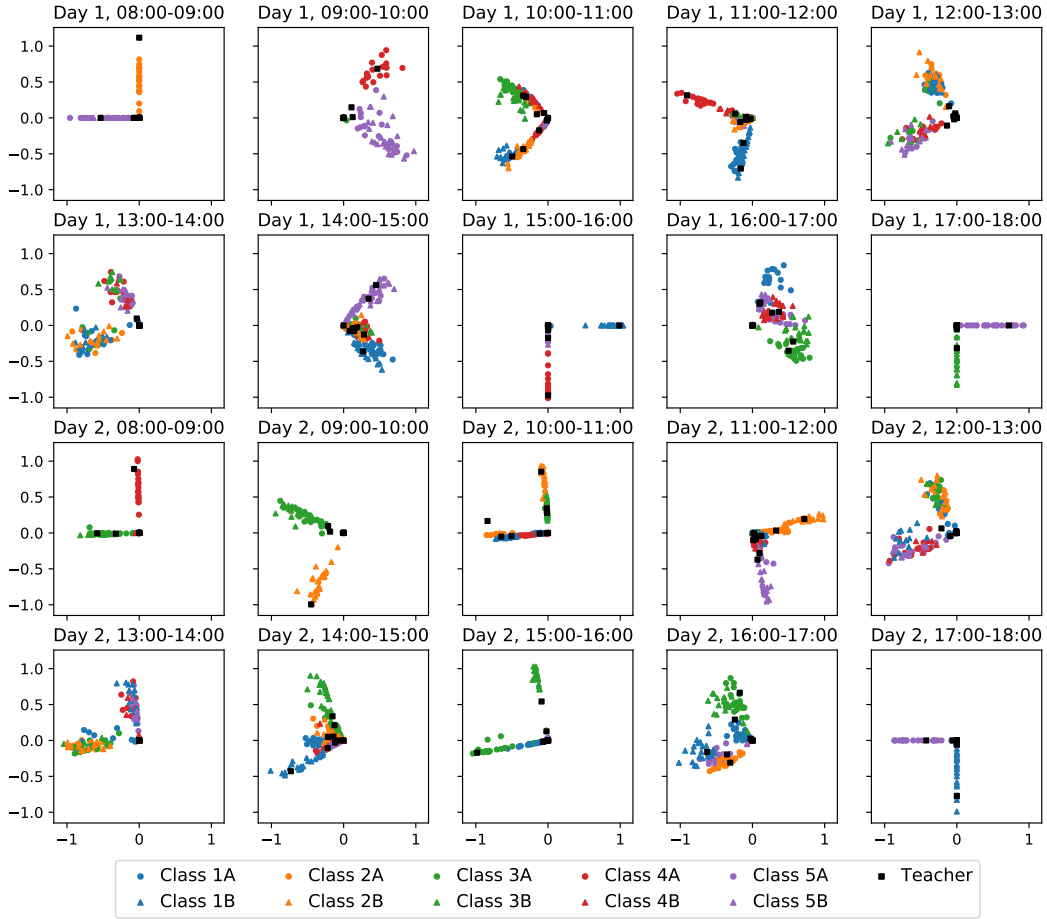


Figure 4: First two dimensions of the embeddings $\hat{\mathbf{Y}}^{(1)}, \dots, \hat{\mathbf{Y}}^{(20)}$ of the adjacency matrices $\mathbf{A}^{(1)}, \dots, \mathbf{A}^{(20)}$. The colours indicate different school years while the marker type distinguishes the two school classes within each year.

From this plot, we see that there is no longitudinal stability using individual adjacency spectral embedding. The classes shown in the leading two dimensions are not the same between time periods. Therefore, we cannot make any inference about how the behaviour of students changes over time.

Secondly, we construct the omnibus matrix $\tilde{\mathbf{A}} \in \mathbb{R}^{nT \times nT}$, where the n -by- n block of the matrix corresponding to times s, t is given by $\tilde{\mathbf{A}}_{s,t} = (\mathbf{A}^{(s)} + \mathbf{A}^{(t)})/2 \in \mathbb{R}^{n \times n}$. We construct the spectral embedding of $\tilde{\mathbf{A}}$ into $\tilde{d} = 10$ dimensions (as with the other embeddings), to obtain $\hat{\mathbf{Y}} \in \mathbb{R}^{nT \times 10}$. This is divided to get the omnibus embedding for each time period, $\hat{\mathbf{Y}} = (\hat{\mathbf{Y}}^{(1)} | \dots | \hat{\mathbf{Y}}^{(20)})$. This takes approximately 30 seconds on a 2017 MacBook Pro. Figure 5 shows the first two dimensions of this embedding to visualise some of the structure in the data.

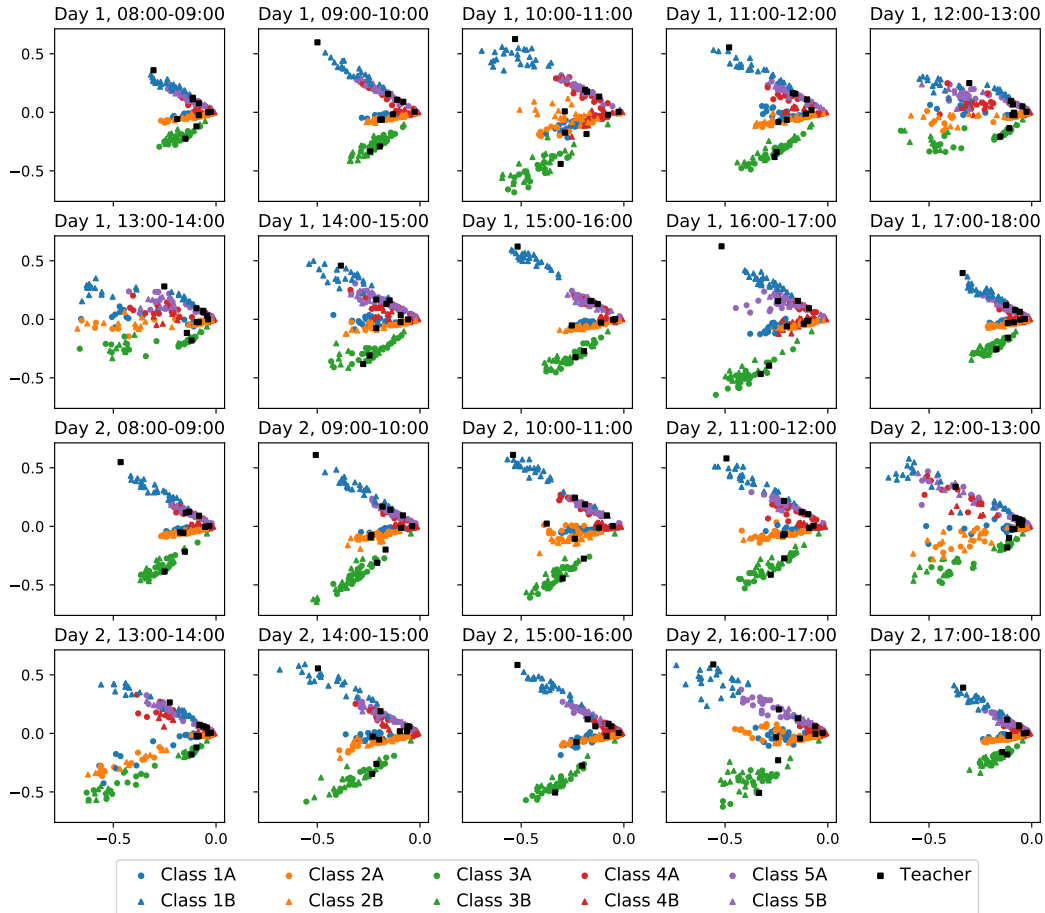


Figure 5: First two dimensions of the embeddings $\hat{Y}^{(1)}, \dots, \hat{Y}^{(20)}$ of the omnibus matrix $\tilde{\mathbf{A}}$. The colours indicate different school years while the marker type distinguish the two school classes within each year.

The rough temporal alignment of the point clouds shows the benefits of omnibus embedding in providing longitudinal stability. However, the lunchtime periods (days 1 and 2, 12:00-14:00) best demonstrate the effect of a lack of cross-sectional stability. Some of the teachers are embedded among what we believe are largely spurious clusters of students during these lunch periods. Empirically, teachers interact much less frequently with students in these periods. Moreover, such a sharp classroom-wise clustering at lunchtime is not present in the independent embedding and seems inconsistent with personal experience. We believe these effects are due to the averaging of past and future behaviours inherent in omnibus embedding, which causes cross-sectional instability.

Lyon primary school data: classification

An alternative use of UASE is to analyse the trajectory of each node through time, in embedded space. Because of the longitudinal stability of UASE, standard multivariate time series analysis techniques can be used to detect trends and seasonal behaviour. These, in turn, could enable latent position forecasting and, from this, link prediction. As background, in such analyses, the time series model is usually incorporated in the embedding process, for example, via a Markov model for the communities [5, 12, 54], or a seasonal autoregressive integrated process on the adjacency matrices [37].

In this section, we instead consider the task of time series classification. Given the trajectory for each student, the goal is to predict their school class. Given an arbitrary time series, this is often done using dynamic time warping [42] or convolutional neural networks [53] to allow for misalignment in

time. However, in this simple example with fixed classroom times, we simply fit a random forest classifier with 100 trees to the concatenation of the spectral embeddings $(\Theta^{(1)} | \dots | \Theta^{(T)}) \in \mathbb{R}^{n \times 9T}$, each using five randomly selected features. The 10-fold cross-validation accuracy is 0.983 ± 0.035 , taking approximately two seconds on a 2017 MacBook Pro.

When classifying a time series in this way, auto-correlation makes feature importance harder to measure. Nevertheless, certain features appear *not* to be important for classification, in particular, we find that the two lunchtime periods (time windows 12:00-13:00 and 13:00-14:00) are not useful, confirming what is shown by those spectral embeddings in Figure 2.

Using this classifier, we can predict the class of the 10 teachers. While we do not expect them to behave exactly as the students, we might hope to match a teacher to their class. Figure 6 shows the proportion of random forest trees classifying each teacher to each school class. Without truth data it is impossible to know if these labels are correct, but the most likely classification assigns exactly one teacher to each class.

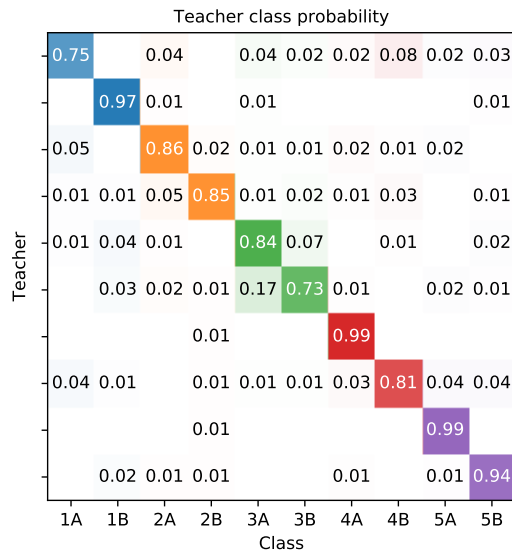


Figure 6: Heat map showing the proportion of random forest trees assigning the spectral embedding trajectory for each teacher to the ten school classes 1A–5B. The colour represents the school class, matching the colours used in Figure 2, where larger proportions are more opaque. Missing values represent a proportion of 0.